Amplitude and phase control of a coherent superposition of degenerate states. I. Theory

Frank Vewinger,* Manfred Heinz,† Bruce W. Shore,‡ and Klaas Bergmann§
Fachbereich Physik der Technischen Universität Kaiserslautern, Erwin-Schrödinger-Straße, 67653 Kaiserslautern, Germany
(Received 15 November 2006; published 25 April 2007)

We present the theory for a technique, based on multistate variants of the stimulated Raman adiabatic passage (STIRAP) process, that allows efficient and robust preparation of a preselected superposition of two or three degenerate states (magnetic sublevels of an atom) and the measurement of their relative amplitudes and phases. Because the preparation utilizes adiabatic passage it is robust against small fluctuations of the Rabi frequencies and temporal shapes of the coupling fields. We here describe and, in the following companion paper we demonstrate, an approach to the experimental characterization of the superposition state, i.e., the measurement of the relative phases and the ratios of amplitudes of the components. That technique, termed phase-to-population mapping, is applicable to the characterization of a stream of identically prepared atoms and is based on laser-induced fluorescence after the atoms have undergone optical pumping cycles induced by an additional laser. The optical pumping process maps the phase into populations of a subset of levels by means of a filtering laser field, and is robust against variations in the intensity and detuning of that field. We describe four linkage patterns appropriate to the creation of superpositions of two or three degenerate states of angular momentum $J=2$, starting from $J=0$. We offer an interpretation, from three different perspectives, of the subsequent characterization procedure.

DOI: 10.1103/PhysRevA.75.043406 PACS number(s): 32.80.Qk, 03.65.Vf, 03.67.Hk

I. INTRODUCTION

Techniques for the preparation and experimental characterization of coherent superpositions of discrete quantum states are crucial to many applications of quantum physics. When the states are nondegenerate, as is the case with molecular vibrational excitation [1] or Rydberg levels [2], the result is a spatial wave packet that moves within a bounded region; the superposition is not stationary in time [3]. When the superposition is degenerate it remains static, i.e., the amplitudes and phases of the constituents are time independent. Such situations are of particular interest for quantum information processing [4] or the preparation of Fock states in a cavity [5].

A portion of this interest in superpositions has centered on trapped atoms [6] or ions [7]; each such atom is addressed individually with carefully crafted pulses that create the desired superposition. Often the techniques rely on variants of π pulses, i.e., excitation in which the time-integrated Rabi frequencies have precisely specified values [7,8]. It has been shown that using such pulses allows one to create arbitrary superpositions of nondegenerate states [9], but the technique described in [9] cannot be extended to degenerate states.

Techniques based on π pulses are of limited use for the preparation of superpositions in atomic beams, because the inevitable distribution of atom velocities produces a corresponding distribution of pulse durations, as experienced by the moving atoms, which leads to, e.g., a reduction of the contrast in Ramsey-Bordé interferometers [10,11]. Instead, beam studies typically rely on some form of adiabatic passage, because these are insensitive to details of the pulsed excitation [12] and allow the creation of superpositions [13] and the preparation of entangled states [14]. By using suitable couplings, and adiabatic passage, one can reach the full Hilbert space spanned by the Zeeman states of a degenerate level [15].

It is important to be able to not only prepare a superposition, but to verify its construction. Equivalently, one must be able to determine the properties (amplitudes and phases) of an unknown superposition. Several techniques for the measurement of the phase between degenerate states as well as their relative amplitudes have been proposed [16,17]. These techniques rely on the measurement of fluorescence after excitation to energetically higher atomic levels with different laser polarizations. Because the radiation characteristics of the fluorescence depend sensitively on the polarization and strength of the exciting laser these proposals are experimentally difficult; they are not robust against fluctuations in the laser parameters.

Our concern is with atoms in a collimated collisionless atomic beam that passes through various cw laser beams. As an atom enters and leaves a laser beam, it experiences a time-dependent pulsed field. The response of the atom to this sequence of time varying fields obeys the time-dependent Schrödinger equation. For a given atom, there is a unique one-to-one connection between spatial position and time, but because atoms have a range of velocities, different atoms experience different pulse durations. Thus for beam excitation, it is desirable to develop techniques that do not require precise adjustment of pulse durations.

An earlier paper described a technique for preparing and characterizing such degenerate superpositions in an atomic beam [18]. The present paper extends that technique to ad-

*Present address: Institut für Angewandte Physik, Wegelerstraße 8, 53115 Bonn, Germany. Electronic address: vewinger@iap.uni-bonn.de
†Present address: AMD Fab36 LLC & Co. KG, Wilschdorfer Landstraße 101, 01109 Dresden, Germany.
‡On leave from: 618 Escondido Circle, Livermore, CA 94550, USA.
§Electronic address: bergmann@rhrk.uni-kl.de

ditional linkage patterns, and provides further details for the measurements of the superposition amplitudes and phases.

The preparation technique is an extension of stimulated Raman adiabatic passage (STIRAP) [19–21], to multistate systems. It allows the preparation of a superposition with predefined relative phases and amplitude ratios within a set of degenerate quantum states. Specifically, the superpositions are of degenerate magnetic sublevels—often termed Zeeman coherences—of quantum states having well-defined angular momentum J. When the laser conditions ensure adiabatic evolution, the resulting superposition is robust against small fluctuations of the Rabi frequencies and temporal shape of the coupling fields.

For the characterization, we here describe a procedure that can fully determine the relative amplitudes and phases of a degenerate superposition. The technique relies on optical pumping of the superposition with a filtering laser, a process that maps the phase onto populations. The full characterization of the superposition is obtained by measuring, as a function of the polarization of the filtering field, the fluorescence from steady-state population of some sublevels after optical pumping.

The paper is organized as follows. First we introduce the different linkage patterns for the creation of the coherent superposition states. We identify related adiabatic dark states, of which one is the desired state for the transfer of population into the superposition. Thereafter, we introduce the concept of phase-to-population mapping and discuss it from three different perspectives.

In a companion paper [22], we describe our experimental setup and results, which we compare to the theoretical predictions of this publication. We thereby demonstrate that this technique allows creation, and subsequent measurement of, not only the relative amplitudes but also the relative phases of the superposition components.

II. STIMULATED RAMAN ADIABATIC PASSAGE WITH DEGENERACY

A. STIRAP linkage

The conventional STIRAP process [20,21] involves three nondegenerate quantum states, having energies $E_1 < E_2$ and $E_3 < E_2$. These undergo excitation by stimulated Raman transitions induced by two pulsed laser fields, P and S, having carrier frequencies ω_P and ω_S, respectively. The carrier frequencies may be detuned from the single-photon resonance with the excited intermediate state 2, but they must together maintain the two-photon resonance condition $\hbar\omega_P - \hbar\omega_S = E_1 - E_3$ between states 1 and 3. The P- and S-laser pulses arrive sequentially, with S preceding (but overlapping with) P. When the time evolution is adiabatic, then this pulse sequence transfers all population from state 1 to state 3, with negligible population in state 2 at any time.

Here, we apply the STIRAP method to transfer population from a single quantum state into a superposition of degenerate states. Specifically, we deal with magnetic sublevels of metastable neon with total angular momentum $J=0$ (initially) and $J=2$ (finally). Figure 1 shows the relevant part of the level scheme of neon, together with the laser excitation

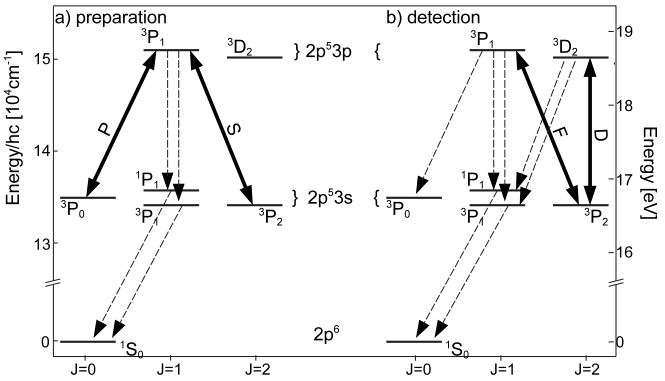

FIG. 1. Energy levels of ^{20}Ne relevant to the experiment. Arrows mark the laser-excitation linkages. (a) Linkages P (pump) and S (Stokes) used during excitation. (b) Linkages F (filtering) and D (detection) used during detection. Dashed lines mark relevant spontaneous emission transitions.

pathways. As shown in Fig. 1(a), the initial state $^3P_0$ is coupled via the P field to three magnetic sublevels of the excited level $^3P_1$, whose lifetime is 18.28 ns [23], i.e., two orders of magnitude shorter than the pulses of ≈ 2.5 μs used in the experiment. The pulse length is determined by the transit time of the atoms through the laser beams. In turn, the S field couples these to the degenerate magnetic sublevels of $^3P_2$; within these the desired superposition is formed. Two other fields, D and F, are required for the detection stage. Figure 1(b) shows these. We take care that, within the region between preparation by the S and P pulses and subsequent action by the F laser, magnetic fields are sufficiently weak that the magnetic sublevels of a given angular momentum J remain very nearly degenerate; this means that the Larmor precession angle for the atom flight between the P and F laser must be much less than π.

B. Rotating wave approximation Hamiltonian

The state vector $\Psi(t)$ representing the system of interest lies in a nine-dimensional Hilbert space, whose basis states we denote as ψ_k, $k=1,\ldots,9$. We take state 1 to be the initial state, the nondegenerate level $^3P_0$ of the $2p^5\,3s$ electronic configuration. We take states 2, 3, and 4 to be degenerate sublevels ($E_2=E_3=E_4$) of the $J=1$ excited level $^3P_1$ of the $2p^5\,3p$ configuration, and we take states 5 through 9 to be degenerate states ($E_5=\cdots=E_9$) of the $^3P_2$ level of $2p^5\,3s$ electronic configuration. It is these latter states that will form the constructed superposition. Figure 2 shows the numbering scheme.

Except for the consequence of radiative decay it is the linkage pattern that matters for the laser excitation dynamics, not the relative ordering of the energies. To make these linkages clear, we place the initial state, state 1, uppermost in the linkage diagrams shown in Fig. 2. This state has energy $E_1 < E_2$, as indicated on the left-hand side of Fig. 2.

We control the relative phases and the ratio of amplitudes of the superposed magnetic sublevels of the $^3P_2$ level by means of a pair of elliptically polarized laser beams, S (Stokes) and P (pump), during a STIRAP-type adiabatic pro-

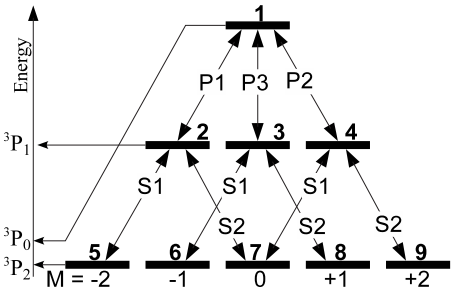

FIG. 2. The linkage pattern and state labels for degenerate angular momentum states considered in this work. Linkages are labeled $S1$ and $S2$ for the two helicity amplitudes of the S laser. The labels $P1$ and $P2$ refer to the helicity amplitudes of the P laser when it is collinear with the S laser, see Fig. 3. The label $P3$ denotes a linkage available when P and S beams are perpendicular and the P beam is linearly polarized in the $\hat{\mathbf{z}}$ direction, see Fig. 4. To the left is an energy scale; light arrows point to the actual energies associated with the levels $J=0$, $J=1$, and $J=2$.

cess. The P-laser field couples the initially populated $J=0$ state to (preselected) sublevels of the $J=1$ level. In turn, the S field couples these to sublevels of the $J=2$ level.

As is customary, we adopt the rotating wave picture and the rotating wave approximation (RWA) [24], writing the state vector as a superposition of the nine bare atomic basis states. Expressing these in a rotating basis we write the construction as

$$\Psi(t) = \sum_n A_n(t)\psi_n(t). \tag{1}$$

The connection between the stationary states ψ_n and the rotating ones $\psi_n(t)$ is

$$\psi_1(t) = \psi_1,$$

$$\psi_{2,3,4}(t) = e^{-i\omega_P t + i\phi_P}\psi_{2,3,4},$$

$$\psi_{5,\ldots,9}(t) = e^{-i\omega_R t + i\phi_S - i\phi_P}\psi_{5,\ldots,9}. \tag{2}$$

The intermediate states rotate with the P-laser frequency, while the target states rotate with the Raman frequency

$$\omega_R = \omega_P - \omega_S. \tag{3}$$

The resulting time-dependent RWA Schrödinger equation reads

$$\frac{d}{dt}A_n(t) = -i\sum_m W_{n,m}(t)A_m(t), \tag{4}$$

where $\hbar W(t)$ is the RWA Hamiltonian matrix. Initially, at time $t=0$, the state vector is taken to be a single state,

$$\Psi(0) = \psi_1. \tag{5}$$

After the conclusion of a STIRAP-like pulse sequence, at time t_f, the state vector is expressible as some combination of states 5 through 9; we write this superposition as

$$\Psi(t) = \sum_{n=5}^{9} |A_n|\exp(i\varphi_n)\psi_n(t), \quad t > t_f, \tag{6}$$

thereby defining the relative phases φ_n and the amplitudes $|A_n|$. Because the states $\psi_n(t)$, $5 \le n \le 9$, are degenerate, they evolve with the same time dependence, i.e., they undergo no wave-packet dynamics. Our objective is to adjust the pulse sequence and polarizations so as to produce a desired set of complex-valued amplitudes $|A_n|\exp(i\varphi_n)$ at time $t=t_f$.

We consider only cases of two-photon resonance (see Fig. 1),

$$\hbar\omega_S - \hbar\omega_P = E_1 - E_9, \tag{7}$$

but we allow for a one-photon detuning Δ,

$$\hbar\Delta = E_2 - E_1 - \hbar\omega_P = E_2 - E_9 - \hbar\omega_S. \tag{8}$$

Thus, the diagonal elements of the RWA Hamiltonian matrix $W(t)$ are

$$W_{11} = W_{55} = W_{66} = W_{77} = W_{88} = W_{99} = 0,$$

$$W_{22} = W_{33} = W_{44} = \Delta. \tag{9}$$

C. Polarization choices

Although the frequency choices dictate the connection $^3P_0 \leftrightarrow {}^3P_1 \leftrightarrow {}^3P_2$, it is the polarization choices which dictate the specific final states that will form the superposition. Here, we discuss the beam geometry and polarizations that provide the desired control.

The P and S fields have electric vectors expressible as products of unit vectors $\hat{\mathbf{e}}_k$, slowly varying envelopes $\mathcal{E}_k(t)$, and carriers at frequencies ω_k,

$$\mathbf{E}_S(t) = \mathrm{Re}[\hat{\mathbf{e}}_S\mathcal{E}_S(t)e^{-i\omega_S t + i\phi_S}], \tag{10}$$

$$\mathbf{E}_P(t) = \mathrm{Re}[\hat{\mathbf{e}}_P\mathcal{E}_P(t)e^{-i\omega_P t + i\phi_P}]. \tag{11}$$

We take the envelope functions to be real valued; the field phases appear explicitly as ϕ_k. The P-field carrier is on or near resonance with the transition between the metastable state $J=0$, and the degenerate excited level with $J=1$, see Fig. 1. The S-field carrier frequency is on or near resonance with the transition between these excited sublevels and the degenerate magnetic sublevels of the metastable level having $J=2$.

We choose the quantization axis $\hat{\mathbf{z}}$ to lie along the propagation direction of the S-laser beam, and express the S-laser electric vector in a helicity basis involving two basis vectors $\hat{\mathbf{e}}_+$ and $\hat{\mathbf{e}}_-$, corresponding to right- and left-circular polarization. These provide the angular-momentum selection rules $\Delta J = \pm 1$ for the linkages between quantum states. In general, both polarization components may be present; it proves convenient to introduce independent amplitudes (with equal time dependence) for the two polarizations, and to write the S field as

$$\hat{\mathbf{e}}_S\mathcal{E}_S(t) = \hat{\mathbf{e}}_+\mathcal{E}_{S1}(t) + \hat{\mathbf{e}}_-\mathcal{E}_{S2}(t)e^{-i2\chi_S}, \tag{12}$$

where $2\chi_S$ is the phase difference between the two polarization components of the S field, i.e., the semimajor axis of the

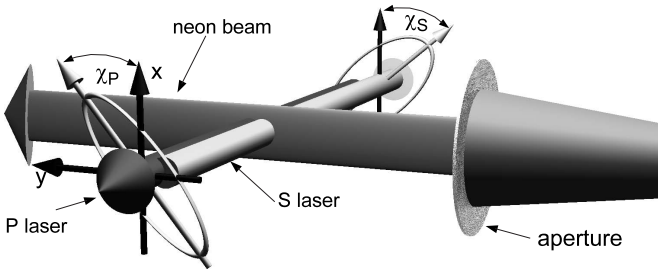

FIG. 3. Experimental setup for the realization of the different coupling schemes. The quantization axis $\hat{\mathbf{z}}$ is chosen to be parallel to the *S*-laser propagation axis. The *P*-laser beam is parallel to the *S* beam; its polarization then must be expressed in a helicity basis, thereby coupling transitions with $\Delta M = \pm 1$.

S-laser polarization ellipse forms an angle χ_S with the x direction (see Fig. 3 or Fig. 4).

The amplitudes of the superposition components are fixed by the amplitudes of the two helicity components of each beam. In turn, these are adjusted by means of quarter-wave plates inserted into the beams. For example, the *S* beam is created with linear polarization in the x direction and amplitude $\mathcal{E}_S$. Upon passing through a quarter-wave plate whose optical axis is oriented at an angle $\theta_{1/4}$ to the x axis the resulting two helicity amplitudes are

$$\mathcal{E}_{S1} = \mathcal{E}_S[\cos\,\theta_{1/4} + \sin\,\theta_{1/4}]/\sqrt{2}, \tag{13}$$

$$\mathcal{E}_{S2} = \mathcal{E}_S[\cos\,\theta_{1/4} - \sin\,\theta_{1/4}]/\sqrt{2}. \tag{14}$$

From the angular-momentum selection rules, it follows that the component $S1$ couples the pairs of states (2,5), (3,6), (4,7), while component $S2$ couples the pairs (2,7), (3,8), (4,9). The nonzero off-diagonal elements $W_{ij}(t)$ of the RWA Hamiltonian $W(t)$ originating from this *S* field are, for $i<j$,

$$\hbar W_{ij}(t) = -\,d_{ij}\mathcal{E}_{S1}(t); \quad \{i,j\} \in \{\{2,5\},\{3,6\},\{4,7\}\},$$

$$\hbar W_{ij}(t) = -\,d_{ij}\mathcal{E}_{S2}(t)e^{-i2\chi_S}; \quad \{i,j\} \in \{\{2,7\},\{3,8\},\{4,9\}\}, \tag{15}$$

The remaining elements, $i>j$, are complex conjugates of these. Here, d_{ij} is the electric-dipole transition moment between states i and j. These incorporate dependence upon magnetic quantum numbers through Clebsch-Gordon coefficients [24,25].

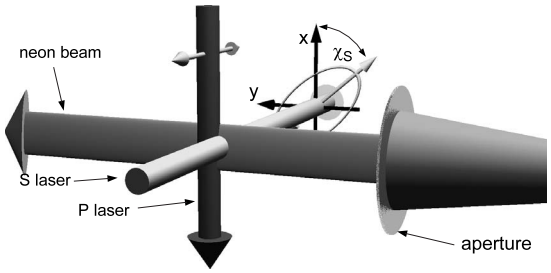

FIG. 4. Experimental setup for the realization of the different coupling schemes. The quantization axis $\hat{\mathbf{z}}$ is chosen to be parallel to the *S*-laser propagation axis. The *P*-laser beam axis is perpendicular to the *S* beam, and it is linearly polarized along the z axis; it couples states for which $\Delta M = 0$.

We will discuss two possibilities for the polarization of the *P* field. These relate to two choices for the propagation direction for the *P* beam. When it is parallel to the *S*-laser beam, see Fig. 3, as for three of the examples discussed below, then the helicity basis is appropriate, and we write the *P* field as

$$\hat{\mathbf{e}}_P\mathcal{E}_P(t) = \hat{\mathbf{e}}_+\mathcal{E}_{P1}(t) + \hat{\mathbf{e}}_-\mathcal{E}_{P2}(t)e^{-i2\chi_P}. \tag{16}$$

Here, as with the *S* field, the phase angle χ_P expresses the rotation of the *P*-field polarization ellipse from the vertical. We adjust this by means of a half-wave plate inserted into the *P* beam. This rotates the angle of polarization by twice its rotation angle, $\chi_S = \frac{1}{2}\theta_{\lambda/2}$.

The helicity components $P1$ and $P2$ couple states (1,2) and (1,4), respectively. The nonzero off-diagonal matrix elements of the RWA Hamiltonian originating with the *P* field are then

$$\hbar W_{12}(t) = -\,d_{12}\mathcal{E}_{P1}(t), \tag{17}$$

$$\hbar W_{14}(t) = -\,d_{14}\mathcal{E}_{P2}(t)e^{-i2\chi_P}, \tag{18}$$

together with complex conjugates.

We orient the *P*-laser beam perpendicular to the *S*-beam axis, see Fig. 4, in order to treat excitation that involves $\Delta M = 0$ linkages. We adjust the *P*-laser polarization to be linear and aligned parallel to the quantization axis, i.e., the *S*-beam propagation axis. With this configuration there occurs only a single polarization component, $P3$. It couples the pair (1,3). Then the only nonzero off-diagonal element from the *P* field is

$$\hbar W_{13}(t) = -\,d_{13}\mathcal{E}_{P3}(t), \tag{19}$$

together with its complex conjugate $W_{31}(t)$.

We express all these RWA matrix elements $W_{ij}(t)$ in terms of the Rabi frequency

$$\Omega = -\,d_{ij}\mathcal{E}/\hbar, \tag{20}$$

where $\mathcal{E}(t)$ is the electric field coupling the transition $i \leftrightarrow j$. Here, the time dependence originates entirely with the slowly varying pulse envelopes $\mathcal{E}_k(t)$. Their time variation is determined by the spatial profile of the laser beams, through the relationship $t = x/v$ for an atom whose longitudinal velocity (perpendicular to the laser beams) is v. Simulation must account for variations in this velocity, as well as Doppler shifts originating in transverse velocity components.

D. Adiabatic evolution

As with conventional STIRAP, the simplest description of the proposed adiabatic evolution into a superposition state is by means of adiabatic states. By definition, adiabatic states are eigenvectors of the RWA Hamiltonian (in the rotating basis),

$$W(t)\Phi_k(t) = \lambda_k(t)\Phi_k(t). \tag{21}$$

We are particularly interested in null-eigenvalue adiabatic states that have no component among states 2–4; these do not undergo loss by spontaneous emission—they are "dark" states [26,27]. These are generalizations of the single dark state of the three-state Raman linkage used in STIRAP. They have the form

$$\Phi^D(t) = A_1(t)\psi_1 + \exp(-i\omega_R t)\sum_{n=5}^{9} A_n(t)\psi_n. \tag{22}$$

As is characteristic for STIRAP, one of the dark states can be chosen such that, prior to the arrival of the S,P pulse sequence at $t=0$, the coefficient $A_1(t)$ has unit magnitude, while after the pulse sequence it has negligible amplitude. We call this state the transfer state.

The N dark states form an N-dimensional subspace of the nine-dimensional Hilbert space. Within this subspace we can choose a basis $\Phi_n^D(t)$, $n=1,N$ for which the diabatic coupling $\langle \dot{\Phi}_k^D(t) | \Phi_\ell^D(t) \rangle$ to the transfer state vanishes, and thus there is no mixing between the degenerate basis states [19]. If the initial state vector $\Psi(t=0)$ is parallel to the transfer state, say $\Psi(t=0) \equiv \Phi_1^D(0)$, it will stay in this state during the adiabatic evolution, i.e., $\Psi(t) \equiv \Phi_1^D(t)$. In this case the adiabatic evolution is completely described by the time evolution of the dark state $\Phi_1^D(t)$.

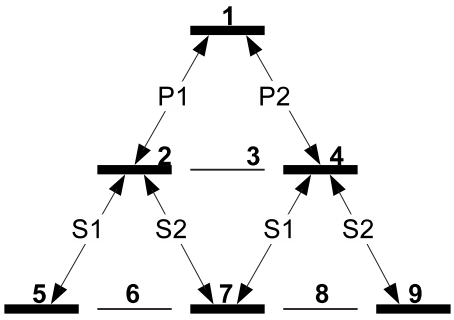

FIG. 5. The linkage pattern associated with circular polarization of P and circular polarization of S; energies are as indicated in Fig. 2. States shown as light lines are either not affected by this radiation or do not participate in the transfer process.

III. EXAMPLES

In the following, we present four specific linkage patterns leading to superpositions of two or three states. A companion paper [22] discusses experimental results for these linkages.

A. Extended diamond STIRAP

The most elaborate linkage pattern we consider occurs when the S- and P-laser beams are collinear, and each is elliptically polarized. Figure 5 shows the resulting linkages.

This linkage allows the construction of a three-state superposition having arbitrary amplitudes and relative phases. The RWA Hamiltonian for this system is

$$W = \frac{1}{2}\begin{bmatrix} 0 & \Omega_{P1} & \Omega_{P2}e^{-i2\chi_P} & 0 & 0 & 0 & 1 \\ \Omega_{P1} & 2\Delta & 0 & b\Omega_{S1} & a\Omega_{S2}e^{-i2\chi_S} & 0 & 2 \\ \Omega_{P2}e^{i2\chi_P} & 0 & 2\Delta & 0 & a\Omega_{S1} & b\Omega_{S2}e^{-i2\chi_S} & 4 \\ 0 & b\Omega_{S1} & 0 & 0 & 0 & 0 & 5 \\ 0 & a\Omega_{S2}e^{i2\chi_S} & a\Omega_{S1} & 0 & 0 & 0 & 7 \\ 0 & 0 & b\Omega_{S2}e^{i2\chi_S} & 0 & 0 & 0 & 9 \end{bmatrix}. \tag{23}$$

The numerical factors a and b incorporate Clebsch-Gordan coefficients for the different transitions [24,25]. We here omit explicit indication of time dependence.

This RWA Hamiltonian has a degenerate two-dimensional dark space. It proves convenient to define the two dark states such that one of the dark states aligns initially with state 1, while the other dark state has no contribution from this state. We take the first dark state of this system to be

$$\Phi_1^D(t) = A_1\psi_1 + e^{-i\omega_R t}[A_5\psi_5 + A_7\psi_7 + A_9\psi_9], \tag{24}$$

where, with normalization factor $\mathcal{N}_1$,

$$A_1 = -ab[b^2\Omega_{S1}^2\Omega_{S2}^2 + a^2(\Omega_{S1}^4 + \Omega_{S2}^4)], \tag{25}$$

$$A_5 = a\Omega_{S1}[b^2\Omega_{P1}\Omega_{S2}^2 + a^2\Omega_{S1} \times (\Omega_{P1}\Omega_{S1} - e^{-2i(\chi_S-\chi_P)}\Omega_{P2}\Omega_{S2})]/\mathcal{N}_1, \tag{26}$$

$$A_7 = a^2 b[e^{2i\chi_P}\Omega_{P2}\Omega_{S1}^3 + e^{2i\chi_S}\Omega_{P1}\Omega_{S2}^3]/\mathcal{N}_1,$$

$$A_9 = a\Omega_{S2}e^{2i(\chi_S+\chi_P)}[b^2\Omega_{P2}\Omega_{S1}^2 - a^2\Omega_{S2} \times (e^{2i(\chi_S-\chi_P)}\Omega_{P1}\Omega_{S1} - \Omega_{P2}\Omega_{S2})]/\mathcal{N}_1. \tag{27}$$

This state incorporates all the coupling with state 1. The other dark state is

$$\Phi_2^D(t) = e^{-i\omega_R t}[A_5'\psi_5 + A_7'\psi_7 + A_9'\psi_9], \tag{28}$$

$$A_5' = ae^{-4i\chi_S}\Omega_{S2}^2/\mathcal{N}_2, \tag{29}$$

$$A_7' = -be^{-2i\chi_S}\Omega_{S1}\Omega_{S2}/\mathcal{N}_2, \tag{30}$$

$$A_9' = a\Omega_{S1}^2/\mathcal{N}_2. \tag{31}$$

Expressions for the two normalization factors $\mathcal{N}_1$ and $\mathcal{N}_2$ are not needed here. The second dark state $\Phi_2^D(t)$ is not involved in the transfer process, because the diabatic coupling between the two dark states vanishes identically, $\langle \dot{\Phi}_1^D | \Phi_2^D \rangle \equiv 0$.

The adiabatic state $\Phi_1^D(t)$ has the property that initially it aligns with ψ_1

$$\Phi_1^D(t) \to \psi_1 \quad \text{when } \sqrt{\Omega_{S1}^2 + \Omega_{S2}^2} \gg |\Omega_{P1}|, |\Omega_{P2}|, \tag{32}$$

and that, upon completion of the pulse sequence, when $|\Omega_{S1}|, |\Omega_{S2}| \ll \sqrt{\Omega_{P1}^2 + \Omega_{P2}^2}$, it becomes a superposition of states 5, 7, and 9. The final state, after the S, P pulse combination, is the superposition

$$\Psi(t) = e^{-i\omega_R t}[A_5\psi_5 + A_7\psi_7 + A_9\psi_9]. \tag{33}$$

The real-valued coefficients A_i and the phases χ_S and χ_P do not change for $t > t_f$. As can be seen from Eq. (28), the two relative phases and two amplitude ratios of the superposition can be controlled independently using the ellipticity and direction of polarization of the S and P field, which gives four controllable parameters. Using the four parameters, the whole Hilbert space spanned by states 5, 7, and 9 can be reached [15].

The populations P_i in the Zeeman levels at the end of the STIRAP sequence can be written, for the simplifying case $\Omega_{P1} = \Omega_{P2}$ and $\Omega_{S1} = \Omega_{S2}$, as

$$P_5 = P_9 = \frac{a^2 + b^2}{2a^2 + b^2} - \frac{b^2}{2[a^2 + b^2 - a^2\cos(2\chi_S - 2\chi_P)]},$$

$$P_7 = \frac{2a^2b^2\cos^2(\chi_S - \chi_P)}{(2a^2 + b^2)[a^2 + b^2 - a^2\cos(2\chi_S - 2\chi_P)]}. \tag{34}$$

This population distribution shows an oscillatory dependence on the relative phase between the P and S fields, which is a manifestation of the interference between the two excitation pathways $1 \to 2 \to 7$ and $1 \to 4 \to 7$, (see also [22]). Due to the different magnitudes of the Clebsch-Gordan coefficients for the pathways leading to state 7 its population is bounded by 1/4, as can be seen by replacing a and b with the appropriate value, $a = 1/\sqrt{3}$ and $b = \sqrt{2}$ [24,25].

B. Extended tripod STIRAP

The three-state superposition of Eq. (28) occurs even when the P field is circularly polarized. Figure 6 shows the linkages for this choice of polarizations.

The RWA Hamiltonian is that of Eq. (23) but without the elements that depend on Ω_{P2}. This RWA Hamiltonian has again a two-dimensional dark space; we take these as in the previous section, Eqs. (24)–(31), with $\Omega_{P2} = \chi_P = 0$.

With the completion of the adiabatic passage, $t > t_f$, the state vector will have the construction

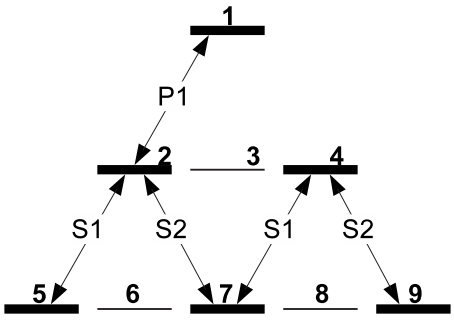

FIG. 6. The linkage pattern associated with circular polarization of P and elliptical polarization of S; energies are as indicated in Fig. 2. States shown as light lines are either not affected by this radiation or do not participate in the transfer process.

$$\Psi(t) = e^{-i\omega_R t}[A_5\psi_5 + |A_7|e^{2\chi_S}\psi_7 + |A_9|e^{4\chi_S}\psi_9]. \tag{35}$$

The phase χ_S is the phase difference between the two Stokes fields, while the three coefficients A_n express the relative amplitudes of the two pulses. With the linkages of Fig. 6, it is not possible to achieve independent control of the relative phase between states 5 and 7 or between states 7 and 9.

C. Twin STIRAP

A simpler situation, producing only a two-state superposition, occurs when the S laser is circularly polarized while the P laser is elliptically polarized. Figure 7 shows the resulting linkage pattern, which we term "twin STIRAP." Because there is only a single helicity component of the S field, we set $\chi_S = 0$.

Only five atomic states are involved, but we retain the numbering of the more complete system shown in Fig. 2. The RWA Hamiltonian matrix is obtained from that of Eq. (23) by omitting elements involving Ω_{S1}.

This RWA Hamiltonian has a single null-eigenvalue adiabatic state. It is

$$\Phi^D(t) = A_1\psi_1 + e^{-i\omega_R t}[A_7\psi_7 + A_9\psi_9], \tag{36}$$

where, with normalization factor $\mathcal{N}$, the coefficients are

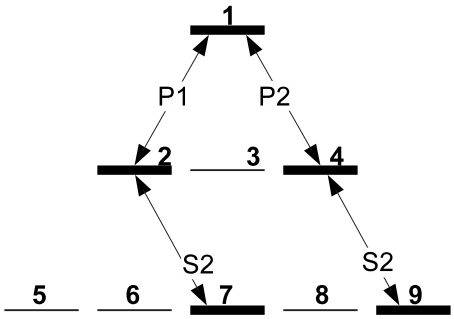

FIG. 7. The twin STIRAP linkage pattern associated with elliptical polarization of P and circular polarization of S; energies are as indicated in Fig. 2. States shown as light lines are not affected by this radiation or do not participate in the transfer process. When the evolution is adiabatic state 8 is not populated by spontaneous emission since states 2 and 4 remain unpopulated. Therefore, the coupling between states 3 and 8 is irrelevant.

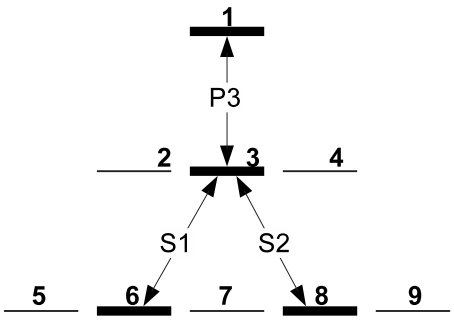

FIG. 8. The linkage pattern associated with linear polarization (z direction) of P and elliptical polarization of S energies are as indicated in Fig. 2. States shown as light lines are either not affected by this radiation or do not participate in the transfer process.

$$A_1 = -ab\Omega_{S2}/\mathcal{N}, \tag{37}$$

$$A_7 = b\Omega_{P1}/\mathcal{N}, \tag{38}$$

$$A_9 = a\Omega_{P2}e^{+i2\chi_P}/\mathcal{N}. \tag{39}$$

This state has the required property that, with the usual STIRAP sequence of S before P, it is initially aligned with the initially populated state 1,

$$\Phi^D(t) \to \psi_1, \quad \text{when } |\Omega_{S2}| \gg \sqrt{\Omega_{P1}^2 + \Omega_{P2}^2}, \tag{40}$$

and that towards the completion of the pulse sequence, when $|\Omega_{S2}| \ll \sqrt{\Omega_{P1}^2+\Omega_{P2}^2}$, it becomes the superposition of only states 7 and 9. Thus, with the completion of the adiabatic passage, the state vector will have the construction of a two-state superposition

$$\Psi(t) = e^{-i\omega_R t}[A_7\psi_7 + A_9\psi_9], \quad t > t_f. \tag{41}$$

The relative phase of the superposition is determined by the relative phase of the P laser helicity components, while the amplitudes $|A_i|$ are determined solely by the ellipticity of the P laser.

D. Tripod STIRAP

The transfer of population from state 1 to the states 6 and 8 requires one transition with $\Delta M = 0$ together with a transition with $\Delta M = \pm 1$. To achieve such transitions it is necessary that the two laser beams are not collinear. This linkage is realized when we orient the P beam to be orthogonal to the S beam, and the linear polarization lies in the $\hat{\mathbf{z}}$ direction (i.e., along the S-beam propagation direction, see Fig. 4). Figure 8 shows the linkages produced by this choice of polarizations [19]. The rows refer to the coupling of the states 1, 3, 6, and 8 (from top to bottom).

Only four states are now involved; we parametrize the RWA Hamiltonian as

$$W = \frac{1}{2}\begin{bmatrix} 0 & \Omega_{P3} & 0 & 0 \\ \Omega_{P3} & 2\Delta & \Omega_{S1} & \Omega_{S2}e^{-i2\chi_S} \\ 0 & \Omega_{S1} & 0 & 0 \\ 0 & \Omega_{S2}e^{+i2\chi_S} & 0 & 0 \end{bmatrix} \begin{matrix} 1 \\ 3 \\ 6 \\ 8 \end{matrix}. \tag{42}$$

This RWA Hamiltonian has a degenerate two-dimensional dark space. We choose the first null-eigenvalue eigenvectors (written in the nonrotating basis ψ_n) to be

$$\Phi_1^D(t) = A_1\psi_1 + e^{-i\omega_R t}[A_6\psi_6 + A_8\psi_8], \tag{43}$$

where, with normalization $\mathcal{N}_1$,

$$A_1 = [\Omega_{S1}^2 + \Omega_{S2}^2]/\mathcal{N}_1, \tag{44}$$

$$A_6 = -\Omega_{P3}\Omega_{S1}/\mathcal{N}_1, \tag{45}$$

$$A_8 = -\Omega_{P3}\Omega_{S2}e^{i2\chi_S}/\mathcal{N}_1. \tag{46}$$

The second dark state, not needed, is

$$\Phi_2^D(t) = e^{-i\omega_R t}[A_6'\psi_6 + A_8'\psi_8], \tag{47}$$

where, with normalization $\mathcal{N}_2$,

$$A_6' = \Omega_{S2}e^{-i2\chi_S}/\mathcal{N}_2, \tag{48}$$

$$A_8' = -\Omega_{S1}/\mathcal{N}_2. \tag{49}$$

The adiabatic state $\Phi_1^D(t)$ has the property that it aligns initially with ψ_1,

$$\Phi_1^D(t) \to \psi_1 \quad \text{when} \quad |\Omega_{S1} + \Omega_{S2}| \gg |\Omega_{P3}|, \tag{50}$$

and that, upon completion of the pulse sequence, when $|\Omega_{S1}+\Omega_{S2}| \ll |\Omega_P|$, it becomes a superposition of states 6 and 8. Thus, with the completion of the adiabatic passage, the state vector will have the construction

$$\Psi(t) = e^{-i\omega_R t}[A_6\psi_6 + |A_8|e^{-i2\chi_S}\psi_8], \quad t > t_f, \tag{51}$$

where the constant coefficients A_6 and A_8 are completely determined by the polarization of the S field.

E. Preparation of superpositions using coherent population trapping

The preceding sections discussed the possibility of preparing superpositions between multiple states using adiabatic transfer, when the two-photon resonance condition is fulfilled. If the laser fields are detuned from the two-photon resonance, the dark states containing state ψ_1 are no longer eigenstates of the system, while the dark states without a contribution from state ψ_1 remain dark states. Thus, a mixture of coherent superposition states within the $^3P_2$ manifold is populated by coherent population trapping (CPT) in the following way: The population of state 1 will be excited to the states 2–4, depending on the polarization of the P laser. Part of that population decays to the states $N=5-9$, where it will either be trapped in the dark states or it will be excited to the states 2–4, from where it may decay back to states 5–9 or to state 1, or to other states outside the level system shown in

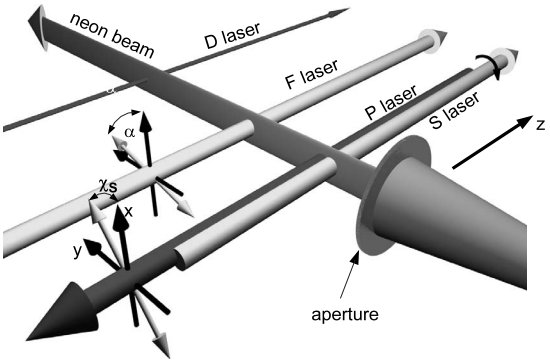

FIG. 9. Geometric layout of the *F*- and *D*-laser beams. Atoms pass first through the *S*-*P* interaction region, then through the *F*-laser beam. This region needs to be essentially free of magnetic fields to ensure degeneracy of the $^3P_2$ manifold and thus avoid Larmor cycling within the Zeeman states.

Fig. 1. After a few cycles of absorbtion followed by spontaneous emission all population will be trapped in a dark state of the system. A comparison of the dark states shown in the former sections reveals that the phases as well as the amplitudes of the prepared superposition in the CPT case differ from the ones in the case of adiabatic transfer. This property can be used for optical phase switching. This has been detailed in [28], and will not be discussed here further.

IV. PHASE-TO-POPULATION MAPPING

As explained in the preceding discussion, one can prepare a variety of superpositions by suitably choosing the polarizations of the two lasers, and then proceeding through a STIRAP-like adiabatic passage that restrains the state vector to remain aligned with a particular adiabatic state. The question remains: how can one verify the successful production of such a superposition, or how can one measure the amplitude ratios and the relative phases for the components of an unknown superposition.

Some populations can be measured quite easily by optical pumping with different polarizations, thereby accessing different components of the population distribution. For example, optical pumping of the transition $J \leftrightarrow J$ with linearly polarized light leaves all population in the state with $M=0$. However, the phases are not accessible by such a straightforward measurement.

Procedures for measuring both amplitudes and phases, by mapping superpositions onto populations of fluorescing excited states, have been described [16,17]. We here present variants of the mapping concept appropriate to the experiments described above and reported in [22].

A. Filtering and detection lasers

We accomplish these measurements by using a combination of a third (filtering) laser *F* and fourth (detection) laser *D* to probe the superposition, as shown in Fig. 9. Atoms pass first through the *S*-*P* interaction region where the superposition is prepared, then through the *F*-laser beam. This region needs to be free of magnetic fields to ensure degeneracy of the Zeeman states. The region between the *F*- and *D*-laser beams does not underly such restrictions.

Both of the *F*- and *D*-laser beams are aligned parallel to that of the *S* laser—the quantization axis for the Zeeman coherences. The polarization of the *D* laser is linear and fixed, while that of the *F* laser is linear with an adjustable angle α measured from the vertical direction (the *x* axis).

Atoms enter the *F*-laser beam in a superposition state, defined with respect to the quantization axis $\hat{\mathbf{z}}$. The *F* laser removes population from the superposition state in a manner dependent on α. Subsequent probing of the remaining population by the *D* laser essentially maps the phase and amplitude distribution of the prepared superposition onto excited-state populations. The strength of the resulting fluorescence signal, as a function of α, provides the needed key to evaluate the superposition amplitudes and phases.

Alternatively, the fluorescence resulting from the excitation with the *F* laser can be measured directly [16,17]. This is experimentally difficult to implement and analyze because only the fluorescence emitted in a limited solid angle $d\Omega$ can be measured using, e.g., a channeltron detector. As the emission characteristics depends on the polarization of the exciting laser the fluorescence is not a direct measure for the populations, but has to be weighted with the direction of the exciting laser. Measuring the populations with an additional *D* laser with a fixed polarization, as in our scheme, overcomes this problem.

In the cases considered here, with linearly polarized *F* laser aligned collinear with the *S* laser, it is only possible to determine the phases between states with magnetic quantum numbers differing by even-integer ΔM. This restriction can be overcome by using an elliptically polarized *F* laser whose direction of propagation forms an angle ϕ with respect to the *S* laser. It has been shown that this configuration allows the measurement of the full density matrix [17].

The combined action of the *F* and *D* lasers can be understood in any one of three different pictures. We term these the optical pumping picture, the dark state picture, and the interferometer picture. The following sections present these explanations.

B. Optical pumping picture

The preceding sections described the preparation of the superposition state using a coordinate system in which the quantization axis $\hat{\mathbf{z}}$ lies along the *S*-laser propagation direction. It proves convenient to regard the direction of the *F*-laser linear polarization as quantization axis $\hat{\mathbf{z}}'$. The connection between the states of angular momentum *J* in the original reference frame (unprimed) $|J,M\rangle$ and (primed) $|J,M'\rangle'$ is provided by the rotation matrix of order *J* [25]:

$$|J,M'\rangle' = \sum_M D^{(J)}_{M',M}(\alpha,\beta,\gamma)|J,M\rangle. \tag{52}$$

The matrix elements $D^{(J)}_{M',M}(\alpha,\beta,\gamma)$ are parametrized using the Euler angles α,β,γ that connect the original and the new reference frame [25]. In our experiment the first Euler angle α is changed, while the second is kept fixed at $\beta=\pi/2$. The third Euler angle does not influence the measurement; it only

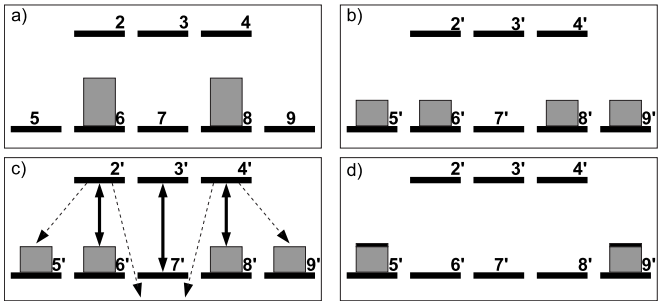

FIG. 10. Principle of the phase-to-population mapping scheme. (a) The initial superposition, with $\pi/2$ given as a sample phase. (b) The population distribution after the rotation of the coordinate system. (c) The F laser acting on the rotated population. Dashed lines show the effect of spontaneous emission. (d) The population after interaction with the F laser. This population, including some from spontaneous emission (dark overlay), is detected by the D laser.

adds an irrelevant phase and can thus be chosen as $\gamma=0$.

In our experiments, the F laser connects the $J=2$ levels of the superposition with an excited level having $J=1$. It is linearly polarized along the rotated quantization axis, and thus it acts only on those states whose magnetic quantum numbers lie between +1 and −1, i.e., the states $6'$, $7'$, and $8'$ of the rotated reference frame. Under the influence of the filtering laser, the system undergoes optical pumping. The populations originally found in states $6'$, $7'$, and $8'$ are, through excitation and subsequent spontaneous emission, entirely removed. They are redistributed, partly into states $5'$ and $9'$ and partly into other states of the atom ($^3P_0$ and the ground state $^1S_0$ via cascade transitions, see Fig. 1), which are not probed. With the neglect of population added to the states $5'$ and $9'$ through optical pumping, we can write their population $S(\alpha)=|A_{5'}|^2+|A_{9'}|^2$ as

$$S(\alpha) = 2\sum_{M<\tilde{M}} [1+(-1)^{M+\tilde{M}}] d^J_{2,M}\left(\frac{\pi}{2}\right) d^J_{2,\tilde{M}}\left(\frac{\pi}{2}\right) C_M C_{\tilde{M}} \times \cos[\alpha(\tilde{M}-M)+(\varphi_M-\varphi_{\tilde{M}})] + 2\sum_M [d^J_{2,M}(\pi/2)]^2 C_M^2. \quad (53)$$

Here, the coefficients C_M bear labels of the magnetic quantum number prior to the rotation of the reference frame; in this reference frame the superposition reads

$$\Psi(t) = e^{-i\omega_R t}\sum_M |C_M(t)|e^{i\varphi_M}|J=2,M\rangle. \quad (54)$$

The summed populations, Eq. (53), exhibits a sinusoidal dependence on α; from the phase of these oscillations one can evaluate the superposition phase. From the amplitude of the signal modulation, one can determine the magnitude of the probability amplitudes. Figure 10 shows the principle of the phase-to-population mapping, interpreted by means of optical pumping.

Following optical pumping induced by the F laser, the atoms travel some 45 cm before reaching the D laser. In that region the magnetic field needs to be sufficiently inhomogeneous and strong to induce Larmor precessions that distribute the remaining population equally among the sublevels $M'=5'\ldots9'$ because of the finite width of the velocity distribution of the beam. Thus, the population in anyone of the M' states is proportional to the population in the states $M'=5'$ and $9'$ after completion of the F-laser-induced optical pumping.

After this Larmor mixing the atoms encounter the D laser. This laser-induces transitions, to another $J=2$ level, whose subsequent spontaneous emission is observed as a fluorescence signal proportional to the total population of all the magnetic sublevels. This signal comprises two components: One from the population which was in states $5'$ and $9'$ before the optical pumping, see Eq. (53), and one from the population which was added as a result of optical pumping of the levels $M'=6'$, $7'$, and $8'$ by the F laser and subsequent spontaneous emission, $P^{op}_{n'}$. The relative weights of these two components vary with the polarization angle α and with the phase angles φ_M; we write the fluorescence signal, proportional to the sum of these populations, as

$$\mathcal{F}(\alpha,\varphi_M) = \eta[P^{op}_{5'}+P^{op}_{9'}+P_{5'}+P_{9'}], \quad (55)$$

where η is the detection probability. The populations $P_{5'}+P_{9'}$ are given by Eq. (53). The terms $P^{op}_{n'}$, which also depend on α and the relative phases φ_M, can be evaluated using numerical simulations. These simulations show that these populations can be neglected if one is only interested in the phase of the superposition, but their knowledge is crucial for the retrieval of the relative amplitudes.

In our experiments, we measure the D-laser-induced fluorescence signal as a function of the angle α, set by the direction of the linear polarization of the F laser. We illustrate the procedure with the example of a coherent superposition created by twin STIRAP. When specialized to the linkage of Fig. 7 the rotation of the coordinates, Eq. (52), has the following consequences for the superposition given by Eq. (41):

$$\begin{matrix}5\\6\\7\\8\\9\end{matrix}\begin{bmatrix}0\\0\\|A_7|\\0\\|A_9|e^{i2\chi_P}\end{bmatrix} \rightarrow \frac{1}{4}\begin{bmatrix}\sqrt{6}|A_7|+|A_9|e^{2i(\alpha+\chi_P)}\\2|A_9|e^{2i(\alpha+\chi_P)}\\-2|A_7|+\sqrt{6}A_9e^{2i(\alpha+\chi_P)}\\2|A_9|e^{2i(\alpha+\chi_P)}\\\sqrt{6}|A_7|+|A_9|e^{2i(\alpha+\chi_P)}\end{bmatrix}\begin{matrix}5'\\6'\\7'\\8'\\9'\end{matrix}. \quad (56)$$

The F laser acts to optically pump all population from states $6'$, $7'$, and $8'$. Thus, the fluorescence subsequently produced by the D laser originates in states $5'$ and $9'$; the signal is

$$\mathcal{F}(\alpha,\chi_P) = \eta[P^{op}_{5'}+P^{op}_{9'}+|A_{5'}|^2+|A_{9'}|^2] = \eta\left(P^{op}_{5'}+P^{op}_{9'}+\frac{1}{8}\left[6|A_7|^2+|A_9|^2+2\sqrt{6}|A_7A_9|\cos(2\alpha+2\chi_P)\right]\right). \quad (57)$$

By monitoring this fluorescence signal as the polarization angle α is varied, we are able to determine the unknown phase χ_P from the phase of the oscillatory term in Eq. (57).

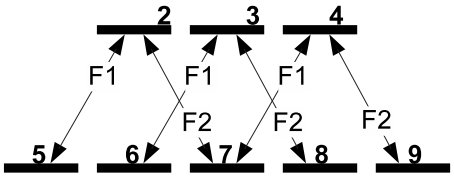

FIG. 11. The couplings of the F laser viewed in the reference system aligned with the S-laser axis.

C. Dark state picture

The concept of phase-to-population mapping may also be viewed in the original coordinate system, wherein the quantization axis relevant for the F-laser interaction remains aligned with the S-laser propagation direction. In that reference frame the F-laser beam is parallel to the quantization axis $\hat{\mathbf{z}}$, and its polarization must be expressed in the helicity representation

$$\hat{\mathbf{e}}_F \mathcal{E}_F(t) = \hat{\mathbf{e}}_+ \mathcal{E}_{F1}(t) + \hat{\mathbf{e}}_- \mathcal{E}_{F2}(t) e^{+i2\alpha}. \tag{58}$$

Here, α is the angle between the x axis and the main axis of the (in general elliptical) polarization of the F laser. Figure 11 shows the coupling scheme of the F laser in this coordinate system.

Analysis of this coupling system reveals two orthogonal dark states

$$\Phi_1^F(t) = \frac{1}{\mathcal{N}_1}[-\Omega_{F2}\psi_6 + \Omega_{F1}e^{+i2\alpha}\psi_8],$$

$$\Phi_2^F(t) = \frac{1}{\mathcal{N}_2}[a\Omega_{F2}^2 e^{-i2\alpha}\psi_5 - b\Omega_{F1}\Omega_{F2}\psi_7 + \Omega_{F1}^2 e^{i2\alpha}\psi_9], \tag{59}$$

where $\mathcal{N}_1$ and $\mathcal{N}_2$ are normalization factors and the factor a and b incorporate the Clebsch-Gordan coefficients. These dark states contain a phase that depends on the angle α, and their relative amplitudes are given by the ellipticity of the F laser.

Population which is in either of these two dark states will be unaffected by the F-laser radiation. The remaining population, residing in bright states, will be removed through optical pumping by the F laser. As a result, the population remaining within the $^3P_2$ level is given by the projection of the superposition state $\Psi(t)$ onto the two dark states, $\Phi_1^F(t)$ and $\Phi_2^F(t)$, i.e., by

$$P_2 = |\langle\Psi(t)|\Phi_1^F(t)\rangle|^2 + |\langle\Psi(t)|\Phi_2^F(t)\rangle|^2. \tag{60}$$

This fraction varies with the angle α and depends on the relative phases φ_n [see Eq. (1)] of the components of the superposition state to be characterized. When α is changed one observes the same variation of the signal $S(\alpha, \chi_S)$, as shown in Eq. (53). This picture of the filter process is especially convenient if the polarization of the F laser is elliptical rather than linear. In this case, our scheme allows not only the measurement of the phases, but also the amplitudes of the given superposition states, if the measurement is done for a number of different ellipticities of the F laser (and thus different ratios $\Omega_{F_1}/\Omega_{F_2}$).

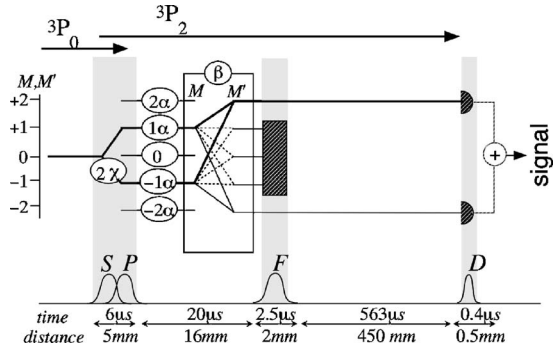

FIG. 12. Schematic representation of the interferometer interpretation of the phase measurement scheme, shown for the example of population transfer by the tripod linkage scheme. Horizontal lines represent Zeeman sublevels; arrows along the top show spectroscopic notation for the energy levels that are populated. The bottom timeline shows the location of the cw laser beams S, P, F, and D. The moving atoms experience these as pulses. Vertical grey bands mark the several interaction regions. In the region between S, P, and F pulses we change the quantization axis; labels change from M to M'. Thick lines connecting $M=0$ at the left to $M'=2$ at the right show one of two interferometer paths; the other path leads to $M'=-2$.

D. Interferometer picture

An interferometric concept is at the heart of any measurement of a phase. Here, we present a qualitative discussion that identifies the various paths which can be viewed as combining to an interferometer for the measurement procedures described in this paper. For the purpose of this discussion, we consider the tripod scheme of Fig. 8.

Figure 12 presents the essentials of the interferometer associated with the amplitude and phase measurements of the two-state superposition associated with this linkage. The figure represents, schematically, a timeline of the effects of the pulse sequence that affects a moving atom or, alternatively, a spatial distribution of events associated with the constant-velocity atom. The horizontal lines of this figure represent magnetic sublevels, labeled $M=-2,\ldots,+2$.

As the atoms enter the apparatus (moving left to right in the figure) they are initially in the $^3P_0$ level (see the topmost labels). The atoms encounter a STIRAP-like pulse sequence, indicated as S and P pulses along the bottom of the figure, and thereby undergo adiabatic transition into two of the five possible magnetic sublevels of the $^3P_2$ level, as indicate along the top of the figure. With the tripod linkage, the two magnetic sublevels have magnetic quantum numbers $M=\pm 1$, in a reference frame aligned with the propagation $\hat{k}_S$ of the S laser; the other sublevels are unpopulated.

The result of the S,P pulse sequence is a coherent superposition of two states, differing in phase by $2\chi_S$, as indicated by the encircled label on one of the two alternative excitation paths. The phase angle χ_S is controlled by the direction of the linear polarization of the S laser relative to the P laser, see

Fig. 3. This step is the beam-splitter portion of the interferometer. When the S laser is linearly polarized the amplitudes of the two states are equal.

The atoms move out of the S,P interaction region and subsequently encounter the F laser, and later the D laser. Vertical grey bands on the figure mark the locations of interactions with the lasers. The F laser beam is parallel to the S and P beams, and has linear polarization oriented at an angle α relative to the linear polarization of the P laser. Therefore, we consider the action of this laser in a rotated reference frame. Prior to the encounter of the atoms with the F laser, we replace the original quantization axis (along $\hat{k}_S$) with an alternative axis rotated by α in a plane perpendicular to $\hat{k}_S$ and then by $\beta=90°$ relative to $\hat{k}_S$. This rotation aligns the new quantization axis along the direction of linear polarization of the F laser. The reorientation, defined by the Euler angles α and β, is not a physical change in the apparatus; it is merely a change of the coordinate system. Thus, the resulting effect can be placed anywhere between the S, P, and F laser interactions. For phase measurement the angle α is varied linearly with time, thereby generating an output that varies sinusoidally with time.

The use of the coordinate system has two consequences. First, it introduces a phase $M\alpha$ to sublevel M, as indicated by encircled labels. Second, it redistributes population among all sublevels: population initially regarded as being in the sublevel having $M=+1$, for example, must be regarded as a coherent superposition of all sublevels, $M'=-2,\ldots,+2$ in the rotated coordinate system. Specifically, the population amplitudes of the states in the rotated frame are given by the rotation matrix elements $D^{(2)}(\alpha,\beta,\gamma)$ with $\gamma=0$, see Sec. IV B.

Having expressed the population distribution by alterations along the timeline, we next discuss the action of the F laser upon these populations. This laser-induces transitions to an excited level and thereby removes all population from sublevels having $M'=-1,0,+1$. The removal is by optical pumping, so some of this population is redistributed, with random phases, into $M'=\pm 2$. However, most of it is lost through spontaneous emission into other levels. The net effect is to leave only population in levels $M'=+2$ and $M'=2$.

It is at this point that we identify the interferometric aspects of the measurement procedure. As indicated by heavy lines in the figure, there are two coherently phased paths that lead from the initial state, $M=0$, to the final state, $M'=+2$. Another pair of paths leads to the final state $M'=-2$. Each of these interferometric paths is independent; the output signal is the sum of the two individual interferometer signals.

During their flight between the S,P interactions and the F pulse, the atoms move through a region in which stray magnetic fields have been made insignificant by applying feedback-controlled compensation fields; thus, there is no field-induced change of the sublevel composition. However, between the F- and D-laser beams there is no such field compensation, and the prevailing magnetic fields there are sufficient to induce Zeeman precession that effectively scrambles the populations and phases.

The atoms then move into the D-laser beam. The resulting excitation produces a fluorescence signal proportional to the total population, i.e., to the sum of the populations left in $M'=\pm 2$ by the F laser.

The output of the interferometer (i.e., the population in $M'=+2$ or $M'=-2$) depends on the initial phase χ_S introduced by the S,P lasers, on the adjustable phase α, and on the fixed angle $\beta=\pi/2$. By varying α we alter the interferometer output from constructive to destructive interference. As is typical of an interferometer, the output signal exhibits a sinusoidal dependence upon α. Therefore, the simultaneous detection of the population $M_\beta=+2$ and $M_\beta=-2$ by the D laser exhibits the sinusoidal variation with α, offset by the phase χ_S, which can thus be retrieved.

Interferometers have, in addition to two interfering paths, two output ports. The population of the $M'=\pm 2$ sublevels leads, upon detection via the D-laser field, to one output port. The other port corresponds to the population of the $M'=-1,0,+1$ sublevels. This is blocked, in the present experiment, by the F-laser optical pumping. Were it not blocked, the D-field detector would have input from both ports of the interferometer, and no modulation would be observable.

V. SUMMARY

We have presented a method that allows the preparation of a superposition of degenerate Zeeman sublevels comprising two or three components, each with a well-defined phase. In particular, the extended diamond STIRAP coupling scheme allows the preparation of an arbitrary but well-defined superposition state of three magnetic sublevels. This coupling scheme also exhibits quantum interference between two pathways. For the preparation of arbitrary two state superpositions we presented twin STIRAP and tripod STIRAP, each addressing different subsets of Zeeman states.

The preparation procedure using adiabatic transfer allows a high degree of flexibility in the choice of amplitudes and phases, and is thus suitable for the manipulation and observation of quantum states where phase control is crucial. Due to its adiabatic nature the preparation is robust against small-to-moderate fluctuations in the Rabi frequencies of the coupling laser fields, allowing its application in experiments where the interaction time is not well defined (as in beam experiments), or the coupling strength of the used transitions is not well known.

We have also presented a scheme for the measurement of the relative phase between the components as well as the ratio of amplitudes. The detection technique described here can be used, quite generally, to measure the superposition phase in a stream of identical systems prepared by any technique.

ACKNOWLEDGMENTS

This work has been supported by the Deutsche Forschungsgemeinschaft. B.W.S. acknowledges support from funds available through the Max Planck Forschungspreis 2003 awarded to K.B. This work was supported by the Marie-Curie Training Network EMALI of the EU.

[1] P. W. Brumer and M. Shapiro, *Principles of the Quantum Control of Molecular Processes* (Wiley, New York, 2003).

[2] J. A. Yeazell, M. Mallalieu, J. Parker, and C. R. Stroud, Phys. Rev. A **40**, 5040 (1989); M. Mallalieu and C. R. Stroud, *ibid.* **51**, 1827 (1995).

[3] T. C. Weinacht, J. Ahn, and P. H. Bucksbaum, Nature (London) **397**, 233 (1999); *Optical Control of Molecular Dynamics*, edited by S. A. Rice and M. Zhao (Wiley-Interscience, New York, 2000); B. M. Garraway and K.-A. Suominen, Rep. Prog. Phys. **58**, 365 (1995).

[4] D. Bouwmeester, A. K. Ekert, and A. Zeilinger, *The Physics of Quantum Information: Quantum Cryptography, Quantum Teleportation, Quantum Computation* (Springer, Berlin, 2000); M. A. Nielsen and I. L. Chuang, *Quantum Computation and Quantum Information* (Cambridge University Press, New York, 2000).

[5] A. S. Parkins, P. Marte, P. Zoller, and H. J. Kimble, Phys. Rev. Lett. **71**, 3095 (1993); A. S. Parkins, P. Marte, P. Zoller, O. Carnal, and H. J. Kimble, Phys. Rev. A **51**, 1578 (1995).

[6] H. J. Briegel, T. Calarco, D. Jaksch, J. I. Cirac, and P. Zoller, J. Mod. Opt. **47**, 415 (2000).

[7] J. I. Cirac, R. Blatt, A. S. Parkins, and P. Zoller, Phys. Rev. A **48**, 2169 (1993); D. Leibfried, R. Blatt, C. Monroe, and D. Wineland, Rev. Mod. Phys. **75**, 281 (2003).

[8] D. Leibfried, E. Knill, S. Seidelin, J. Britton, R. B. Blakestad, J. Chiaverini, D. B. Hume, W. M. Itano, J. D. Jost, C. Langer, R. Ozeri, R. Reichle, and D. J. Wineland, Nature (London) **438**, 639 (2005); A. Ben-Kish, B. DeMarco, V. Meyer, M. Rowe, J. Britton, W. M. Itano, B. M. Jelenkovic, C. Langer, D. Leibfried, T. Rosenband, and D. J. Wineland, Phys. Rev. Lett. **90**, 037902 (2003).

[9] C. K. Law and J. H. Eberly, Opt. Express **2**, 368 (1998).

[10] Ch. Lisdat, M. Frank, H. Knöckel, M.-L. Almazor, and E. Tiemann, Eur. Phys. J. D **12**, 235 (2000).

[11] Ch. J. Bordé, Ch. Salomon, S. Avrillier, A. van Lerberghe, Ch. Bréant, D. Bassi, and G. Scoles, Phys. Rev. A **30**, 1836 (1984).

[12] K. Bergmann, H. Theuer, and B. W. Shore, Rev. Mod. Phys. **70**, 1003 (1998).

[13] A. R. Karapetyan and A. D. Gazazyan, Laser Phys. **11**, 655 (2001); R. G. Unanyan, B. W. Shore, and K. Bergmann, Phys. Rev. A **63**, 043401 (2001); L. P. Yatsenko, N. V. Vitanov, B. W. Shore, T. Rickes, and K. Bergmann, Opt. Commun. **204**, 413 (2002); R. G. Unanyan, M. E. Pietrzyk, B. W. Shore, and K. Bergmann, Phys. Rev. A **70**, 053404 (2004); Y. Niu, S. Gong, R. Li, and S. Jin, *ibid.* **70**, 023805 (2004); S. Gong and Y. Niu, Opt. Spectrosc. **99**, 270 (2005); A. Karpati and Z. Kis, J. Phys. B **36**, 905 (2003); E. S. Kyoseva and N. V. Vitanov, Phys. Rev. A **73**, 023420 (2006); N. V. Vitanov, K.-A. Suominen, and B. W. Shore, J. Phys. B **32**, 4535 (1999).

[14] R. G. Unanyan, B. W. Shore, and K. Bergmann, Phys. Rev. A **63**, 043405 (2001); R. G. Unanyan, N. V. Vitanov, and K. Bergmann, Phys. Rev. Lett. **87**, 137902 (2001).

[15] Z. Kis, N. V. Vitanov, A. Karpati, C. Barthel, and K. Bergmann, Phys. Rev. A **72**, 033403 (2005).

[16] N. V. Vitanov, B. W. Shore, R. G. Unanyan, and K. Bergmann, Opt. Commun. **179**, 73 (1999); N. V. Vitanov, J. Phys. B **33**, 2333 (2000).

[17] P. Ivanov and N. V. Vitanov, Opt. Commun. **264**, 368 (2006); C. Barthel, Z. Kis, U. Schneider, and K. Bergmann (unpublished).

[18] F. Vewinger, M. Heinz, R. Garcia-Fernandez, N. V. Vitanov, and K. Bergmann, Phys. Rev. Lett. **91**, 213001 (2003).

[19] R. Unanyan, M. Fleischhauer, B. W. Shore, and K. Bergmann, Opt. Commun. **155**, 144 (1998).

[20] N. V. Vitanov, T. Halfmann, B. W. Shore, and K. Bergmann, Annu. Rev. Phys. Chem. **52**, 763 (2001).

[21] N. V. Vitanov, M. Fleischhauer, B. W. Shore, and K. Bergmann, Adv. At., Mol., Opt. Phys. **46**, 55 (2001).

[22] F. Vewinger, M. Heinz, U. Schneider, C. Barthel, and K. Bergmann, following paper, Phys. Rev. A **75**, 043407 (2007).

[23] S. A. Kandela and H. Schmoranzer, Phys. Lett. **86A**, 101 (1981).

[24] B. W. Shore, *The Theory of Coherent Atomic Excitation* (Wiley, NewYork, 1990).

[25] R. N. Zare, *Angular Momentum: Understanding Spatial Aspects in Chemistry and Physics* (Wiley, New York, 1988).

[26] E. Arimondo, in *Progress in Optics* (Elsevier Science, Amsterdam, 1996), Vol. XXXV, p. 257.

[27] R. G. Unanyan, K. Bergmann, and B. W. Shore, Phys. Rev. A **59**, 2910 (1999).

[28] M. Heinz, F. Vewinger, U. Schneider, L. P. Yatsenko, and K. Bergmann, Opt. Commun. **264**, 248 (2006).